Research of the defect structure and colouring mechanism of black lithium tantalate wafers

QINGYAN XU[1,2,4], JIASHUN SI[1,2,3], SHUAIJIE LIANG[1,2,3], YAN ZHANG[1,2,3], YAN HUANG[1,2,3], LINGLING MA[1,2,3], LIANG HAI[1,2,3], XUEFENG ZHANG[1,4], MENGFAN WANG[5], HUAN ZHANG[1,2,3], XUEFENG XIAO[1,2,3,*]
[1]*College of Electric and Information Engineering, North Minzu University, Yinchuan, 750021, China*
[2]*Key Laboratory of Physics and Photoelectric Information Functional Materials Sciences and Technology, North Minzu University, Yinchuan, 750021, China*
[3]*Microelectronics and Solid-State Electronics Device Research Center, North Minzu University, Yinchuan, 750021, China*
[4]*Ningxia Ju Jing Yuan Crystal Technology Company Limited, Shizuishan 753000, China*
[5]*School of Materials Science and Engineering, Zhengzhou University, Zhengzhou, 450001, China*

In this work, a chemical reduction method has been used to prepare black lithium tantalate (BLT) wafers. The defect structure and chromogenic mechanism of BLT wafers were investigated. It was found that the reduction process results in the reduction of a large amount of Ta^{5+} to Ta^{4+}, and a small percentage of low valence $Ta^{3+/2+}$ ions to Ta^{4+} or Ta^{5+} on the surface of lithium tantalate wafers. At the same time, it produced a large number of O vacancies. The O vacancies and structural distortion of TaO_6 were the main reasons for the blackening of lithium tantalate wafers.

(Received December 18, 2023; accepted April 8, 2024)

Keywords: Black lithium tantalate, Defect structure, Colouring mechanism, O vacancies

1. Introduction

Lithium Tantalate ($LiTaO_3$, LT) crystal is a multi-functional crystal material with excellent piezoelectric, photoelectric and pyroelectric properties [1-3]. It is widely used to make surface wave filters (SAW) due to its large piezoelectric coefficient and low insertion loss [4]. Due to its high pyroelectric coefficient and optical transmittance, the surface can easily collect a large amount of electrostatic charge at high temperatures, which can lead to device damage. Meanwhile, high light transmittance reduces the yield of devices affecting wafer lithography [5].

Researchers have proposed a chemical reduction method for the preparation of black low-static LT wafers to solve the problem of low yield and damage to the device from accumulated electrostatic charges in the fabrication of SAW devices. In 2011, Zhang et al. used zinc and silicon powders to reduce LT wafers, and the reduced wafers were red-brown in color [6]. The reduced LT wafers were also known as black lithium tantalate (BLT) wafers. The transmissivity of BLT wafers under 325 nm light are reduced to 35% of unreduced LT wafers. After reduction, the resistivity of LT chip changes from 5.28×10^{14} Ω·cm reduced to 2.83×10^{10} Ω·cm, piezoelectric performance has not changed much. Long et al. studied the thermal conductivity and thermal expansion coefficient of BLT chips [7]. The thermal conductivity of LT wafer is 2.79 W/(m·K) and the thermal expansion coefficient is $6.94\times10^{-6}K^{-1}$, while the thermal conductivity of BLT wafer is 2.66W/(m·K) and the thermal expansion coefficient is 2.79×10^{-6} K^{-1}. The reduction in the coefficient of thermal expansion has reduced the temperature drift coefficient of SAW devices and the yield of the devices has improved considerably. Zhang Xianhong et al. gave the reason for the decrease of pyroelectric coefficient of BLT crystals [5]. The lower resistance of BLT wafers compared to LT wafers results in less static charge build-up and thus lower pyroelectric coefficients. In conclusion, the resistivity, thermal conductivity, transmittance and thermal expansion coefficient of BLT crystals are lower than LT crystals while the reduction of resistivity, transmittance and thermal expansion coefficient is beneficial to the fabrication and performance of SAW devices. It improves the performance and yield of SAW devices. Therefore, BLT wafers are more suitable for making SAW devices than LT wafers.

In 1985, L. A. Kappers et al. studied the infrared spectra and low temperature Electron Spin Resonance (ESR) spectra of LT wafers after annealing [8]. The LT wafers became darker after annealing in a high temperature argon atmosphere and the transmittance of the LT wafers in the infrared spectrum at 460 cm^{-1} increased due to annealing. The ESR spectroscopy demonstrated that a defect has trapped an electron in the Ta ion within the crystal, resulting in a change from Ta^{5+} to Ta^{4+}, providing side evidence of O vacancies within the LT crystals. In 2011, Yan Tao et al. tested the X-ray diffraction patterns (XRD) and X-ray energy spectra (XPS) of BLT wafers and concluded that the lattice parameters of BLT wafers were slightly reduced [9]. The Ta4f electron layer and O1s electron layer energy spectra of the XPS of BLT wafers were analysed, yielding Ta inversion defects on the wafer surface. The change in valence of the Ta ion from +5 to +4

is the main reason for the change in colour of the wafers and presumes O vacancies on the wafer surface. The surface morphology, electrical, thermal and mechanical properties of BLT wafers have also been investigated by our group, [10, 11] and it was concluded that the annealing and wafer reduction environments have a significant impact on the quality of BLT wafers. The O-element content of the BLT wafers surface will be reduced and the surface roughness will be reduced. The electrical and thermal properties of the reduced LT wafer will be improved while the mechanical properties will be reduced.

Although researchers have studied the surface morphology, defect structure and physical properties of BLT wafers, there is no direct evidence of O vacancies within BLT wafers. The mechanism for the darkening of the LT wafer after reduction remains to be investigated. In this work, BLT wafers were prepared using a chemical reduction method and the internal defect structure and colour-causing mechanism of BLT wafers were investigated. The effects of different processes on the surface stress of BLT wafers were obtained using Raman spectroscopy and Raman imaging. The Ta and O ion valence states and optical transmittance within BLT crystals have been studied using X-ray photoelectron spectroscopy and infrared spectroscopy, and direct evidences of O vacancies within BLT crystals have been obtained. A new mechanism for the colour change of BLT wafers is proposed, providing the necessary reference for the theoretical study of BLT crystals and their applications.

2. Experimental

2.1. Preparation of black lithium tantalate wafer

LT crystals were grown using the pull-down method and LT crystal rods were cut into thin slices with a wafer orientation of Y42°. The wafers #1 and #3 were annealed at 580 °C and the wafer #2 was not annealed. Reduction of wafers #2 and #3 was carried out in a home-made vacuum furnace at a vacuum of 10^{-2}Pa, using silicon and aluminium powders as reducing agents. The specific process of reduction is shown in the literature [11]. Fig. 1 shows the prepared BLT wafer. As can be seen in Fig. 1, the wafer #1 is the lightest in colour and the wafer #3 turns completely black. Both annealing and blackening will darken the wafer while only LT wafers that have undergone both annealing and blackening will be completely black in colour. XRD was tested on all chips and found no other heterojunction except for $LiTaO_3$ [11, 12].

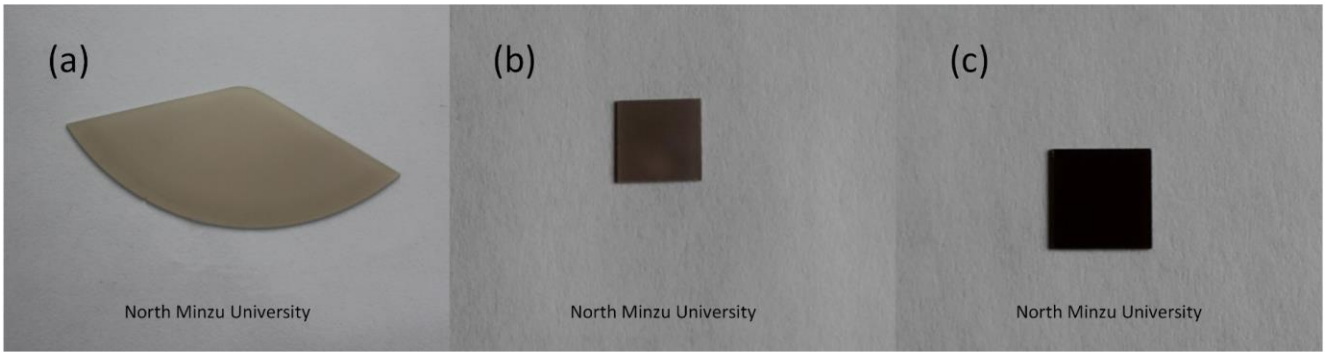

Fig. 1. The images of LT wafers (a) #1 (b) #2 (c) #3

2.2. Raman Spectroscopy Testing

The Raman spectra of the samples were tested using an inViaTM laser confocal micro-Raman spectrometer from Renishaw. During the experiments, all samples were tested under the same conditions using a 532 nm laser with an exposure time of 10 s and scanning in the range of 100-1000 cm^{-1}.

2.3. X-ray photoelectron spectroscopy (XPS) testing

Raman imaging was also tested using an InViaTM laser confocal micro-Raman spectrometer from Renishaw. The target peaks were imaged by sequentially acquiring 4800 Raman spectra in an array of 1 μm steps within a selected 80 μm × 60 μm area. The 4800 acquired Raman spectra were subjected to uniform cosmic ray removal and fitting batches of imaging peaks using analysis software, and then the fitted spectral peaks were subjected to microscopic Raman imaging. All samples were tested under the same conditions.

2.4. Raman imaging testing

The XPS spectra of all LT samples were measured using a Thermo Fisher Scientific k-Alpha X-ray photoelectron spectrometer. The radiation source was an Al K alph source with a test energy of 1486.8 eV. The test

spot area was 30-500 μm and all samples were tested under a vacuum of 2×10^{-9} mbar.

2.5. Infrared spectroscopy testing

Infrared spectroscopy spectra of #1 and #3 LT wafers were tested using PerkinElmer Spectrum Two. Uses a high temperature mid-infrared (MIR) light source with an infrared laser wave number of 11750 cm^{-1} and a scanning wave number range of 450-4000 cm^{-1}.

3. Results and discussions

3.1. Raman spectroscopy analysis

Raman spectroscopy can reflect the internal defects, chemical bonds and ion concentration of crystals. Fig. 2 shows the Raman spectra of wafers #1, #2 and #3. As can be seen from Fig. 2, both wafers #1 and #2 have twelve Raman peaks, with wafer #2 having a higher Raman peak intensity than #1. The wafer #3 has eleven Raman peaks, 863 cm^{-1} less than the wafers #1 and #2. In terms of Raman activity, a defect-free LT crystals should have 13 Raman peaks [13]. The lack of Li ions in the LT crystals result in a large number of intrinsic defects in the crystal. These intrinsic defects result in the absence of the Raman peaks of wafers #1 and #2. While the wafer #3 was annealed and blackened, the annealing and blackening process resulted in the wafer #3. The Raman peak at 863 cm^{-1} is missing from the wafer. Analysis of the number of Raman peaks for wafers #1, #2 and #3 show that annealing and then blackening of the LT wafers also reduces the number of Raman peaks. From the overall Raman spectra, it can be seen that the position and half-peak width of the Raman peaks change after reduction of the LT wafer, which is due to the change in defect structure and atomic concentration inside the BLT wafer [14].

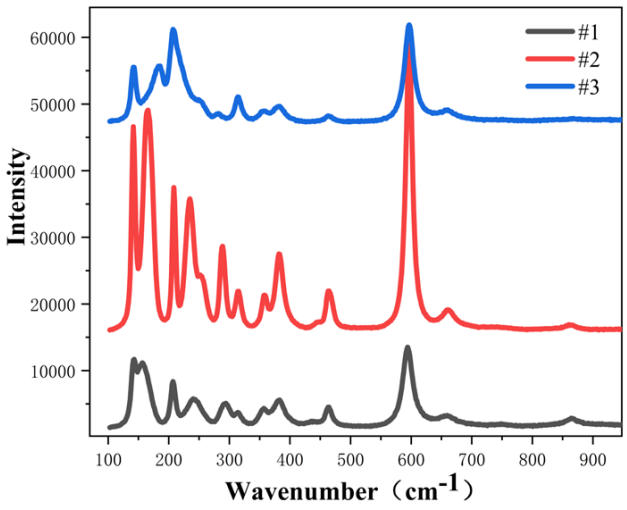

Fig. 2. Raman spectra of LT crystals (color online)

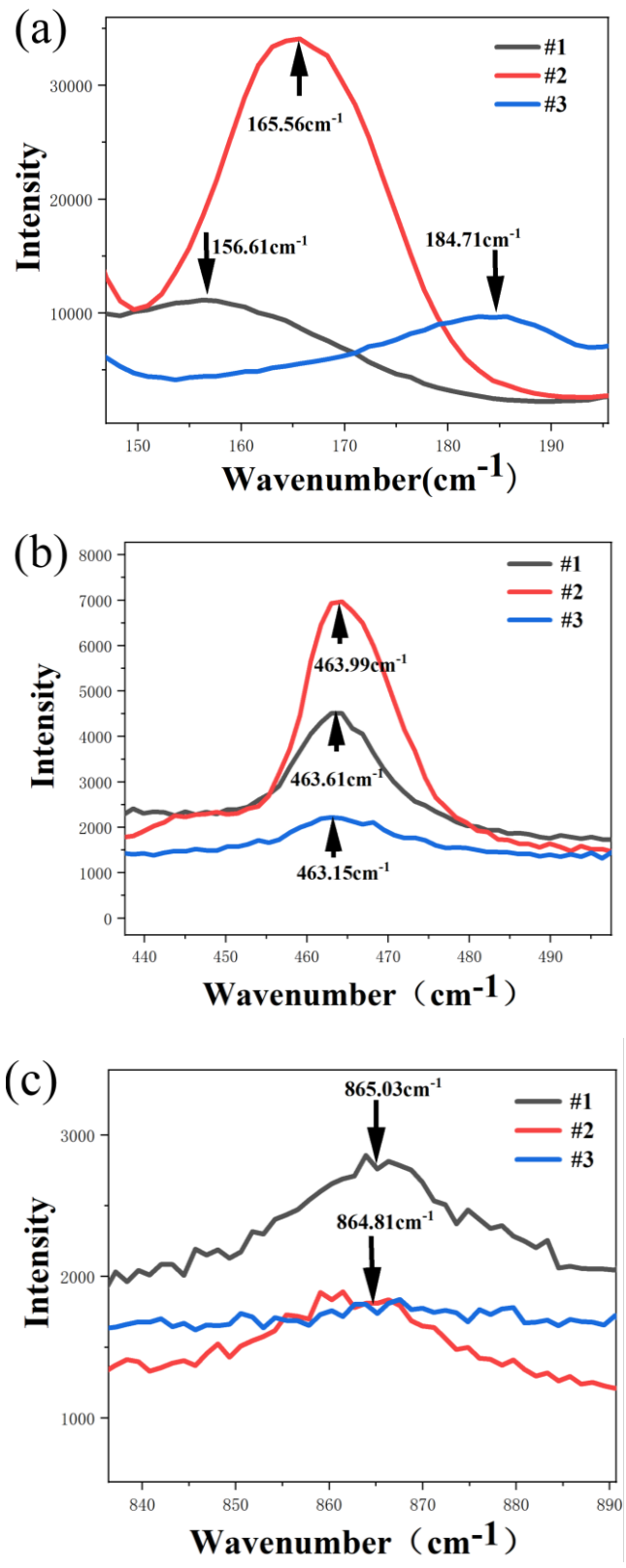

Fig. 3 . Localised Raman peaks of LT crystals (a) 160 cm^{-1} (b) 460 cm^{-1} (c) 863 cm^{-1} (color online)

Fig. 3 shows a comparison of the local Raman peaks of the LT wafers, where Fig. 3(a) shows a comparison of

the Raman peaks of wafers #1, #2 and #3 near 160 cm^{-1}. From Fig. 3(a), the Raman peaks for wafers #1, #2 and #3 are 156.61 cm^{-1}, 165.56 cm^{-1} and 184.71 cm^{-1}. The Raman peaks of wafer #2 and #3 here are both redshifted relative to #1 wafer, and wafer #3 is more redshifted. The Raman peaks for the three samples here were fitted using the Gauss-Lorentz function in Origin, giving peak half-peak widths of 27.99 cm^{-1}, 16.96 cm^{-1} and 15.54 cm^{-1} respectively. The Raman peak here is associated with the Ta ion within the LT crystals [15]. The red shift of the Raman peak indicates a change in the valence state of the Ta ion, while the decrease in the half-peak width indicates a decrease in the concentration of Ta-related defects or lattice relaxation of some Ta ions. Fig. 3(b) shows the Raman peaks around 460 cm^{-1} for the three samples with Raman peaks of 463.61 cm^{-1}, 463.99 cm^{-1} and 463.15 cm^{-1} respectively. The peaks of different wafers here are almost unchanged. After Gauss-Lorentz fitting, the Raman peak half-peak widths of wafers #1, #2 and #3 here are 12.56 cm^{-1}, 14.33 cm^{-1} and 19.36 cm^{-1} respectively, which show an increasing trend. The Raman peak at 460 cm^{-1} is associated with the O ion [15]. Since both annealing and reduction are carried out under oxygen less or oxygen free conditions, annealing and reduction can result in LT wafers with O vacancy defects. Fig. 3(c) shows a comparison of the Raman peaks around 863 cm^{-1} for samples #1, #2 and #3. The wafers #1 and #2 have peaks of 865.03 cm^{-1} and 864.81 cm^{-1} respectively, while the #3 wafer has essentially no Raman peak here. The Raman peak half width is reduced in #2 compared to #1 wafer, while the Raman peak at 863 cm^{-1} is largely lost in the annealed and reduced wafer #3. The Raman peak at 863 cm^{-1} correlates with the internal stress in the LT crystals [12]. Therefore, the Raman peak on the annealed and reduced wafer #3 disappears here, also indicating that there is less stress inside the wafer at this point.

To sum marise, we suggest that the Raman peak at 160 cm^{-1} in the Raman spectrum of the LT wafers are related to Ta ion movement and valence changes. The Ta ion becomes lower in valence and the Raman summit here is red-shifted. The Raman peak half-peak width at 460 cm^{-1} correlates with the concentration of O vacancies. The Raman peak near 863 cm^{-1} is related to the stress and strain within the wafer and less to intrinsic defects within the crystals. These points were again verified in the following Raman imaging and XPS analysis.

3.2. Raman imaging analysis

Raman imaging can analyse the stress and strain distribution on the crystal surface, so we have performed Raman imaging of the stress and strain related peaks at 865 cm^{-1} of the wafers. Fig. 4 shows the Raman peak intensity imaging around 865 cm^{-1} for all wafers. As can be seen from Fig. 4(a), the Raman peak intensities of sample #1 is not uniformly distributed, and the peak intensities show an overall trend of convergence, with peak intensities ranging from 246-654. This indicates an uneven distribution of atoms and defects on the surface of sample #1. From Fig. 4(b), it can be seen that the wafer #2 has a relatively uniform distribution of Raman peak intensities at 865 cm^{-1}, but is stratified, with peak intensities ranging from 2300-2440. This indicates that sample #2 was overstressed internally during the reduction process, leading to the creation of internal twin boundaries. The presence of twin boundaries leads to an uneven distribution of stresses on the surface and the increase in Raman peak intensity indicates other defects on the wafer surface. From Fig. 4(c), it can be seen that the Raman peak intensity of wafer #3 at 865 cm^{-1} is more uniformly distributed, and there is no stratification phenomenon, and the peak intensity range is 544-1248. This indicates a uniform stress distribution on the surface of the wafer #3.

Imaging of Raman peak widths and peak positions around 865 cm^{-1} for the three samples are shown in Fig. 5 and Fig. 6. As can be seen from Fig. 5, the peak width imagings of both wafers #2 and #3 have more a uniform distribution than that wafer #1, indicating that the reduction in the preparation process can result in a more uniform stress distribution on the wafer surface. As can be seen from Fig. 6, the distribution of pixel dots in the Raman peak position imaging of sample wafer #1 is not uniform, with the three colours having distinct areas of pixel dot distribution and a tendency for the same pixel dots to converge. However, the #2 and #3 Raman peak positions have a uniform distribution of pixel points, but the wafer #2 wafer has significant delamination. In summary, annealing mainly reduces internal stresses in the wafer, reduction allows for a more even distribution of surface stresses, and reduction causes some defects on the wafer surface.

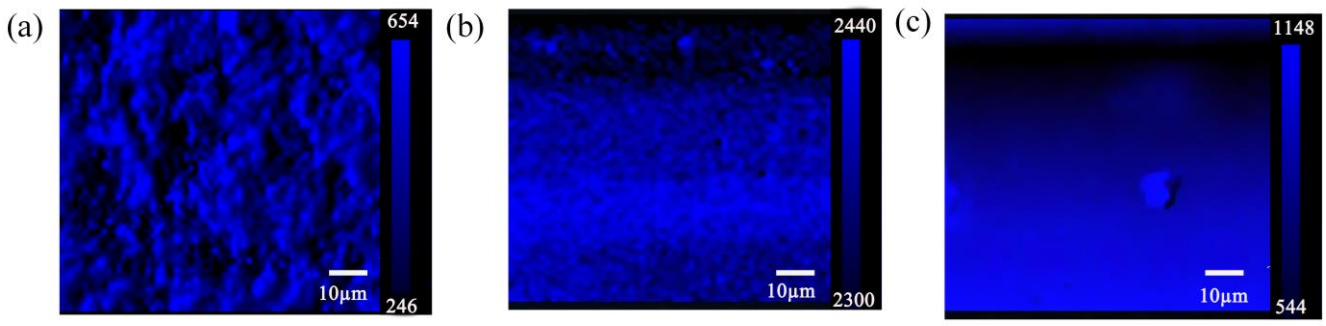

Fig. 4 . Raman peak intensity imaging of LT wafer at 865 cm^{-1} (a) #1 (b) #2 (c) #3 (color online)

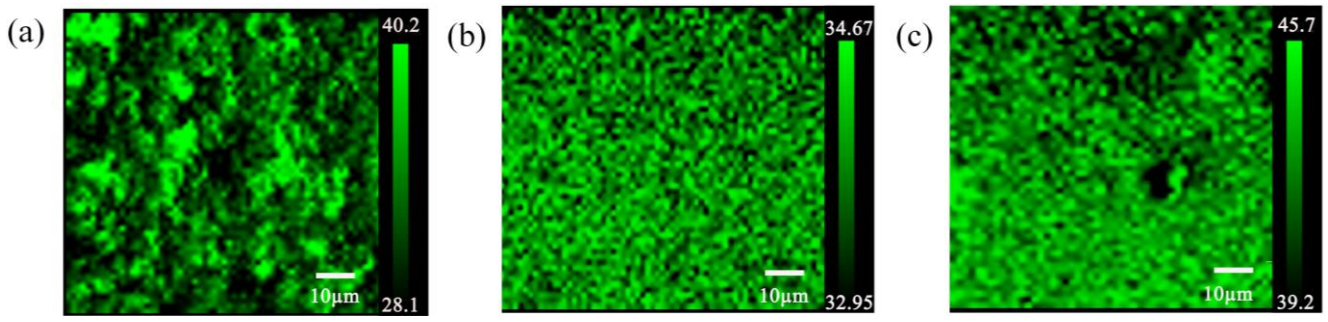

Fig. 5. Raman peak width imaging of LT wafer at 865 cm^{-1} (a) #1 (b) #2 (c) #3 (color online)

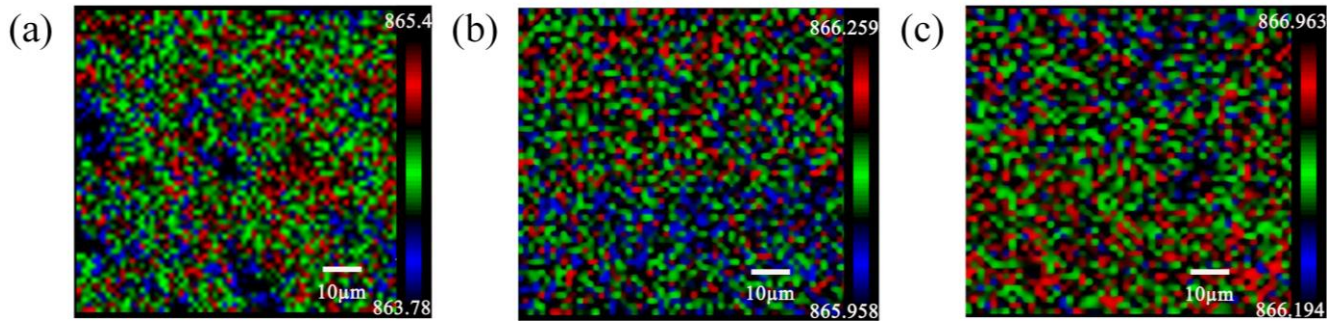

Fig. 6. Imaging of the Raman peak position of the LT wafer at 865 cm^{-1} (a) #1 (b) #2 (c) #3 (color online)

3.3. X-ray energy spectroscopy (XPS) analysis

In order to investigate the defects produced on the surface of BLT wafers and the mechanism of wafer color change, the XPS energy spectra of wafers #1 and #3 were tested. The number of atoms on the surface of wafers #1 and #3 are shown in Table 1. As can be seen from Table 1, the percentage of O and Ta on the surface of the wafer #1 is greater than wafer #3, while the percentage of Li atoms is lower than the wafer #3. The main reason for these experimental results is that during the reduction process for wafer #3, the reduction caused the escape of O atoms from the LT wafer surface. The more O is lost, the higher the concentration of O vacancies on the wafer surface. When the LT wafers are exposed to high temperatures, Li ions diffuse to the surface, resulting in more Li atoms on the surface of the BLT wafers than the LT wafer. Therefore, the colour changes of the wafers are related to the change of the atomic concentration percentage on the wafer surfaces.

Fig. 7 shows a comparison of the XPS energy spectra of the Ta4f electron layers of wafers #1 and #3. From Fig. 7(a), the peak Ta4f electron layer binding energy of wafer #1 is greater than #3. From the above, it can be seen that the Ta ion valence state on the surface of BLT wafers is different from LT wafers. Fig. 7(b) and Fig. 7(c) show the peak splitting fits for the Ta4f electron layers of wafers #1 and #3. Based on the binding energy corresponding to the valence state [12], it can be seen that wafer #1 has 75% Ta^{5+}, 13.31% Ta^{4+} and 11.69% Ta in the lower valence state. In contrast, the #3 sample had 43.74% Ta^{5+} and 56.26% Ta^{4+}. This indicates that Ta^{5+} on the surface of BLT crystals was reduced to Ta^{4+} during the reduction process for sample #3, which is consistent with the conclusion reached by Yan T et al. [9]. The difference is that the internal low-valent Ta ion disappears and transforms into Ta^{4+} or Ta^{5+}.

Table 1. LT wafer surface elemental composition table

	O percentage（%）	Ta percentage（%）	Li percentage（%）
#1	57.02	27.17	15.81
#3	50.99	15.45	33.57

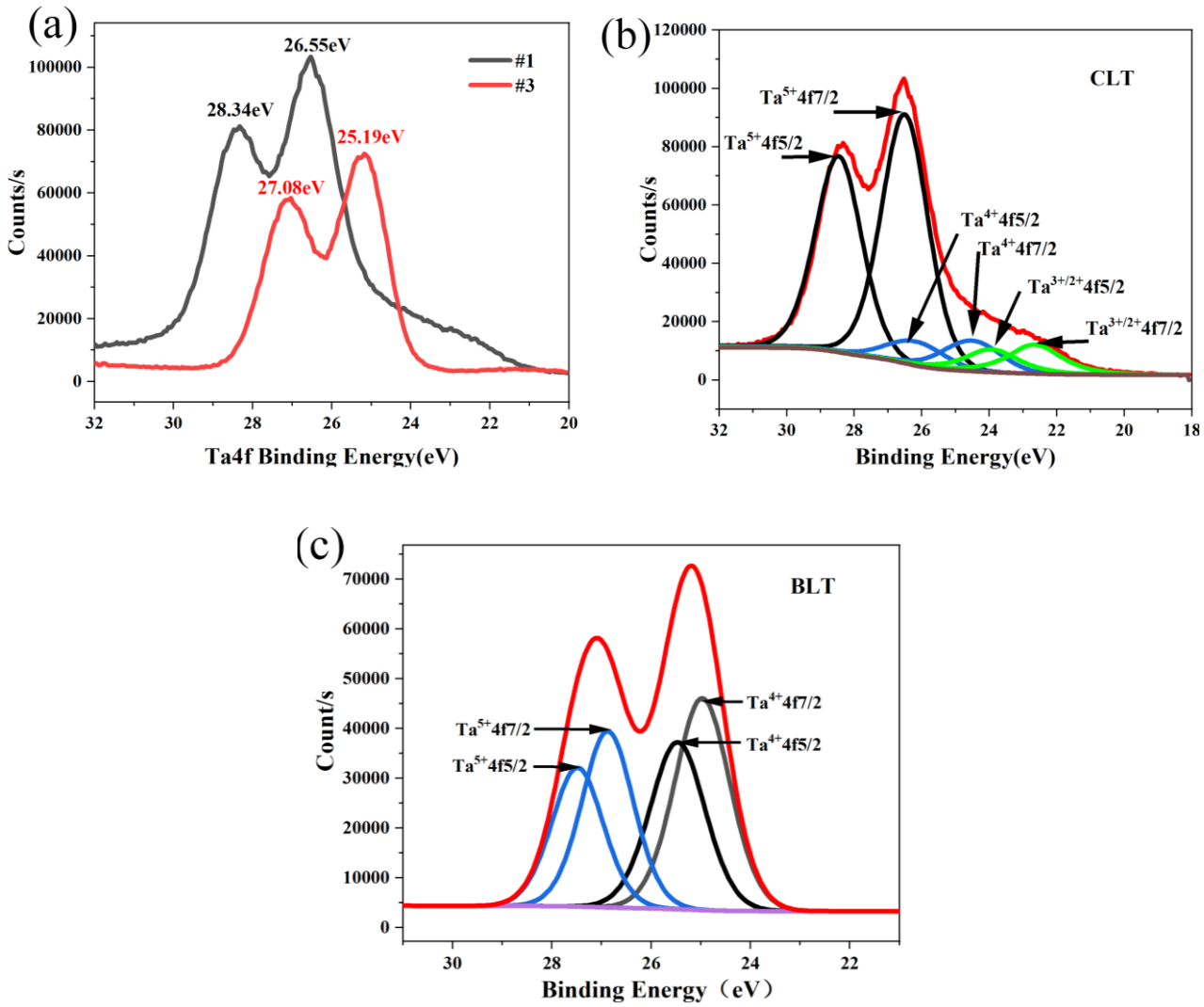

Fig. 7. XPS energy spectra (a) Comparison of Ta4f electron layer energy spectra of #1 and #3 wafers (b) Fitting of Ta4f electron layer splitting on #1 wafer (c) Fitting of Ta4f electron layer splitting on #3 wafer (color online)

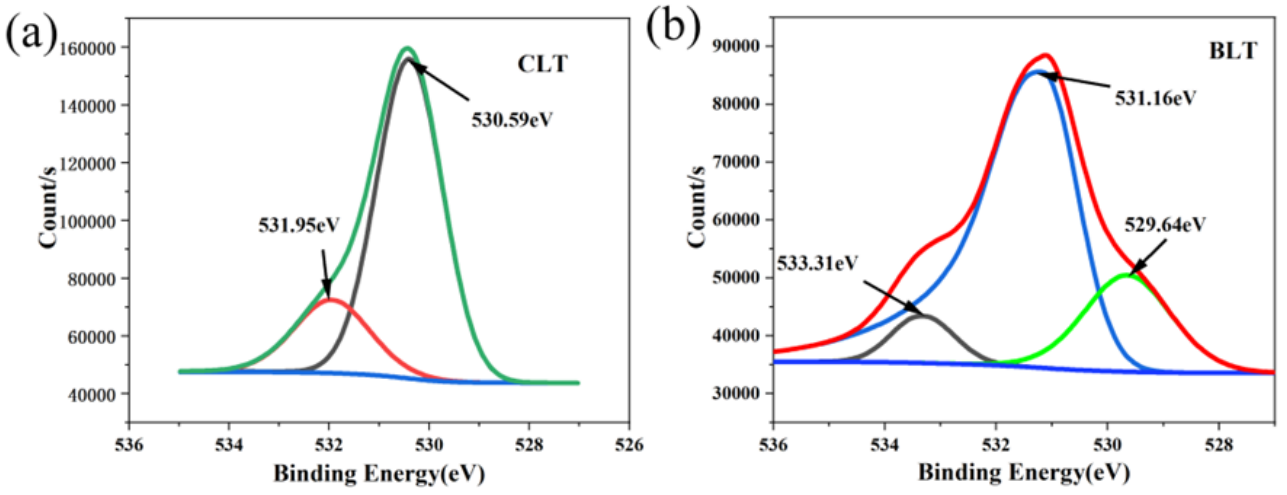

Fig. 8. Fitting of O1s electron layer splitting (a) #1 (b) #3 (color online)

Fig. 8 is the peak fitting diagram of O1s electronic layer of # wafers #1 and # 3. As can be seen from Fig. 8, the O1s electron layer of wafer #1 was fitted by two single peaks with binding energy peaks of 530.59 eV and 531.95 eV. The O1s electron layer of wafer #3 was fitted by three single peaks with binding energy peaks of 529.63 eV, 531.16 eV and 533.31 eV. This indicates that the reduction process resulted in an increase in the O1s electron binding energy of the BLT crystal, with a peak binding energy of 533.31 eV single peak after peak fitting. This single peak is the binding energy corresponding to the O vacancies, [16, 17] so the BLT wafer surface produces O vacancies. Yan T et al. [9] also speculated that BLT wafers contain O vacancies, but the O1s fraction of their BLT wafers did not give a binding energy peak of 533.31 eV which is directly related to O vacancies. This may be related to the reducing agent used in the wafer reduction or the length of the reduction process. This is because different reducing agents may have different reduction effects and there are cases of incomplete and inadequate reduction. In addition, the longer the same reducing agent reduces the wafer under vacuum, the more O is lost and the higher the O vacancy concentration. A combination of Raman spectroscopy and XPS energy spectroscopy of the O1s energy spectrum leads to the conclusion that there are O vacancy defects on the surface of the BLT wafer.

3.4. Infrared spectral analysis

Fig. 9 shows the Infrared (IR) spectra of wafers #1 and #3. From Fig. 9(a), most of the IR light transmission rates of wafer #3 is lower than wafer #1, indicating that the reduction process significantly reduces the IR light transmission. Fig. 9(b) shows the local IR spectra of wafers #1 and #3, with peaks at 300-800 cm^{-1} dominated by 459.99 cm^{-1} and 514.67 cm^{-1} for #1 and 461.94 cm^{-1} and 507.72 cm^{-1} for #3. After reduction of the LT wafer, the transmission peak at 459.99 cm^{-1} is red-shifted and the transmission peak at 514.67 cm^{-1} is blue-shifted on the IR spectrum. The IR spectrum at 513 cm^{-1} is associated with NbO_6 octahedra [18, 19]. The LT crystals also have TaO_6 inside, so the transmission peak at 514.99 cm^{-1} where the LT wafer appears in the infrared spectrum is associated with TaO_6. At the same time, the concentration of O vacancies increases and the transmission peak on the IR spectrum is red-shifted, [20, 21] so that the peak at 460 cm^{-1} in the IR spectrum is mainly associated with O vacancies [8].

Reduction leads to an increase in the concentration of O vacancy defects within the crystal. The increase in O vacancies leads to a local distortion of TaO_6, resulting in a red-shift of its peak in the IR spectrum and a decrease in light transmission. The colour of the substance itself is related to the light it absorbs and the electron leap of the ions inside it. LT crystals do not have chromogenic ions inside them, so it is mainly related to the absorption and transmission of light by the crystal [22]. An increase in the concentration of O vacancy defects leads to enhanced absorption of visible light by the wafer, [23] so the absorption of visible light by BLT wafers mainly comes from O vacancy defects and structural distortion of TaO_6.

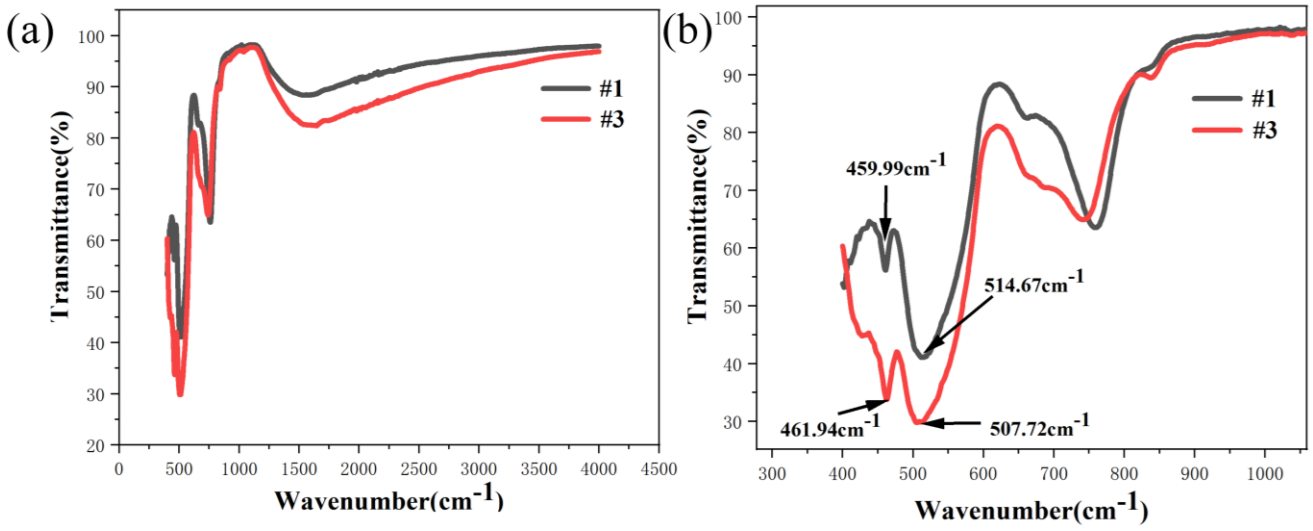

Fig. 9. IR spectra of wafers #1 and #3 (a) IR spectra (b) Local IR spectra (color online)

4. Conclusions

BLT wafers were prepared by chemical reduction method. The effects of annealing and reduction processes on the stress distribution and defect structure of BLT wafers were investigated, and the mechanism of colour change of BLT wafers was studied. The stresses on the surface of LT wafers were analysed using Raman

spectroscopy and Raman imaging, and it was found that the internal stresses in the annealed LT wafers are reduced and that the stresses are more evenly distributed after reduction. The Raman peak at 160 cm^{-1} in LT crystals is related to the Ta ion position and valence state, while the Raman peak at 863 cm^{-1} is mainly related to the internal stress of the wafer and less to the intrinsic defect concentration in LT crystals.

The XPS spectra of LT wafers and BLT wafers were fitted to the binding energy of the Ta4f and O1s electron layers, resulting in the reduction of some of the Ta^{5+} to Ta^{4+} and the valence of the remaining low valence Ta ions to Ta^{4+} or Ta^{5+} after the reduction of the LT wafers. A large number of O vacancy defects can be created in the wafer. The infrared spectroscopy analysis of LT and BLT chips shows that the transmittance peak near 514.99 cm^{-1} of LT wafers is related to TaO_6, and the main factors affecting the infrared and visible light transmission of BLT wafers are O vacancy defects and TaO_6 structural distortion. Therefore, the colour change in BLT wafers is mainly due to a combination of O vacancy defects and TaO_6 structural distortion.

Acknowledgments

This research was funded by the Fundamental Research Funds for the Central Universities, North Minzu University (2020DXXY002 and 2021KJCX07), the National Natural Science Foundation of China(61965001 and 11864001), the Ningxia Province Key Research and Development Program (2018BEE03015, 2021BEE03005, 2021BDE932020 and 2022BFE02009), the Natural Science Foundation of Ningxia(2019AAC03103), the Ningxia first-class discipline and scientific research projects (electronic science and technology) (NXYLXK2017A07). The Ningxia Central Leading Local Science and Technology Development Special Project (2021FRD05009). The authors thank the Ningxia new solid electronic materials and Devices research and development innovation team, the Ningxia advanced intelligent perception control innovation team and the Ningxia acoustooptic-crystals industrialization Innovation team.

References

[1] J. G. Gualtieri, J. A. Kosinski, A. Ballato, IEEE Trans. Ultrason. Ferroelectr. Freq. Control **41**, 53 (1994).
[2] A. Hossain, M. H. Rashid, IEEE Trans. Ind. Appl. **27**, 824 (1991).
[3] K. F. Chen, Y. L. Li, C. Peng, L. Zheng, X. Y. Luo, D. F. Xue, Inorg. Chem. Front. **8**, 4006 (2021).
[4] M. Kadota, Y. Ishii, S. Tanaka, J. Appl. Phys. **61**, SG1041 (2022).
[5] X. H. Zhang, Y. G. Chen, Y. Zhu, S. Q. Chen, Piezoelectrics & Acoustooptics **39**, 797 (2017).
[6] X. F. Zhang, B. Zhang, W. T. Zhou, Mater. China **30**, 58 (2011).
[7] Y. Zhou, M. X. Yu, H. X. Li, Z. B. Shi, L. Wang, Y. C. Ding, Y. Xu, Z. G. Wu, Piezoelectrics & Acoustooptics **41**, 340 (2019).
[8] L. A. Kappers, K. L. Sweeney, L. E. Halliburton, J. H. Liaw, Phys. Rev. B **31**, 6792 (1985).
[9] T. Yan, F. F. Zheng, Y. G. Yu, S. B. Qin, H. Liu, J. Y. Wang, D. H. Yu, J. Appl. Crystallogr. **44**, 158 (2011).
[10] X. F. Xiao, Q. Y. Xu, H. Zhang, L. L. Ma, L. Hai, X. F. Zhang, Optoelectron. Adv. Mat. **16**(7-8), 364 (2022).
[11] X. F. Xiao, H. Zhang, X. F. Zhang, J. Mater. Sci. Mater. Electron. **31**, 16414 (2020).
[12] X. F. Xiao, Q. Y. Xu, S. J. Liang, H. Zhang, L. L. Ma, L. Hai, X. F. Zhang, J. Mater. Sci. Mater. Electron. **33**, 20668 (2022).
[13] S. Sanna, S. Neufeld, M. Rüsing, G. Berth, A. Zrenner, W. G. Schmidt, Phys. Rev. B **91**, 224302 (2015).
[14] J. E. Sosa Márquez, L. Zamarrón Montes, S. F. Olive-Mendez, J. Am. Ceram. Soc. **105**, 5956 (2022).
[15] Y. Repelin, E. Husson, F. Bennani, C. Proust, J. Phys. Chem. Solids **60**, 819 (1999).
[16] S. A. Abdullah, M. Z. Sahdan, N. Nayan, Z. Embong, C. R. C. Hak, F. Adriyanto, Mater. Lett. **263**, 127143 (2020).
[17] Z. L. Wang, L. Z. Wang, EcoMat. **3**(1), e12075 (2021).
[18] T. Belin, N. Guigue-Millot, T. Caillot, D. Aymes, J. C. Niepce, J. Solid State Chem. **163**, 459 (2002).
[19] R. Li, L. Y. Liu, B. M. Ming, Y. H. Ji, R. Z. Wang, Appl. Surf. Sci. **439**, 983 (2018).
[20] Q. Y. Hou, S. Q. Guo, C. W. Zhao, Acta Phys. Sin. **63**, 283 (2014).
[21] J. B. Kang, Z. X. Fang, X. Chen, W. Liu, F. Y. Guo, S. T. Wu, Y. F. Yong, J. Z. Chen, J. Alloys Compd. **599**, 170 (2014).
[22] T. Li, G. J. Zhao, X. M. He, J. Xu, S. K. Pan, J. Synth. Cryst. **31**, 456 (2002).
[23] Z. Zhang, I. A. Rusakova, J. Wilson, R. Chu, W. K. Chu, Instrum. Meth. B **127**, 515 (1997).

*Corresponding author: xuefengxiao@nmu.edu.cn